Windborne debris trajectories in tornado-like flow field initiated from a low-rise building

Bourriez, Frederick; Sterling, Mark; Baker, Christopher

DOI:
10.1016/j.jweia.2020.104358

Document Version
Peer reviewed version

Citation for published version (Harvard):
Bourriez, F, Sterling, M & Baker, C 2020, 'Windborne debris trajectories in tornado-like flow field initiated from a low-rise building', *Journal of Wind Engineering and Industrial Aerodynamics*, vol. 206, 104358. https://doi.org/10.1016/j.jweia.2020.104358

Windborne debris trajectories in tornado-like flow field initiated from a low-rise building

Frederick Bourriez [a], Mark Sterling [a], Chris Baker [a]

[a] *University of Birmingham, School of Engineering, Edgbaston, Birmingham, U.K.*

ABSTRACT: This paper examines compact debris flight in tornado-like flow fields. The research focuses on physically simulating a specific tornado-like vortex and on investigating windborne debris flight with and without a low-rise building model. The low-rise building model, $1/8^{th}$ scale with regard to the vortex core radius, was used to initiate the flight of Styrofoam spheres from its top. Debris motion was recorded using three high-speed cameras and data reduction was performed on open-source OpenPTV software. Flow field characterisation showed that including a building model does not considerably affect the averaged flow field but only the local instantaneous flow field. Debris flight analysis shows that the mean flight distance is not affected by the building model, but a change in the initial direction occurs. Comparison between local wind flow field and initial debris velocities shows good agreement, and therefore the variability in initial directions of the debris flight can be attributed to a wind-driven process. To compare with experimental data, experimental data were incorporated into debris flight equations to compute debris motion. Debris trajectories computed from experimental data show strong visual similarities with experimental trajectories and debris flight analysis presents good agreement with experimental data.

KEYWORDS: tornado-like vortex, debris, low-rise building, 3D-PTV.

1 INTRODUCTION

Tornadoes are fast vertical swirling columns of air formed inside a storm and connecting the cloud base and the ground via a funnel cloud. Tornadoes account for the strongest and most devastating natural wind phenomenon with wind speeds up to 480 km/h. When fully developed, the width of a tornado can reach half a mile in diameter and travel long distances. Moreover, the debris cloud during a tornadic event, observable when dust and/or objects are lifted aloft and are swirling around the tornado, can account for twice the size of the tornado itself (Wurman *et al.*, 2013). In 2018, 628 tornadoes were reported in Europe. In the United Kingdom, about 30 tornadoes are reported every year, with 2.2 tornadoes per year per 10,000 km sq. on average. This is more than in the U.S. with 1.3 tornadoes per year per 10,000km sq. and about 1,200 tornadoes occurring every year (Mulder and Schultz, 2015). Nevertheless, tornadoes in the U.S. are stronger than tornadoes usually occurring in Europe. As a result, over the last 40 years, about 60 fatalities were reported and billions of dollars of damages are caused every year on U.S. soil. Damage to property and infrastructure due to tornadoes can mainly be attributed to the high wind speeds, the low pressure inside the vortex core and windborne debris (Brooks and Doswell, 2001). Windborne debris embedded during strong wind events, such as downbursts, hurricanes or tornadoes, can lead to major wind disasters. When reaching high velocities, debris can significantly damage engineered and non-engineered buildings, resulting in the production of even more debris, known as debris chain (Figure 1).

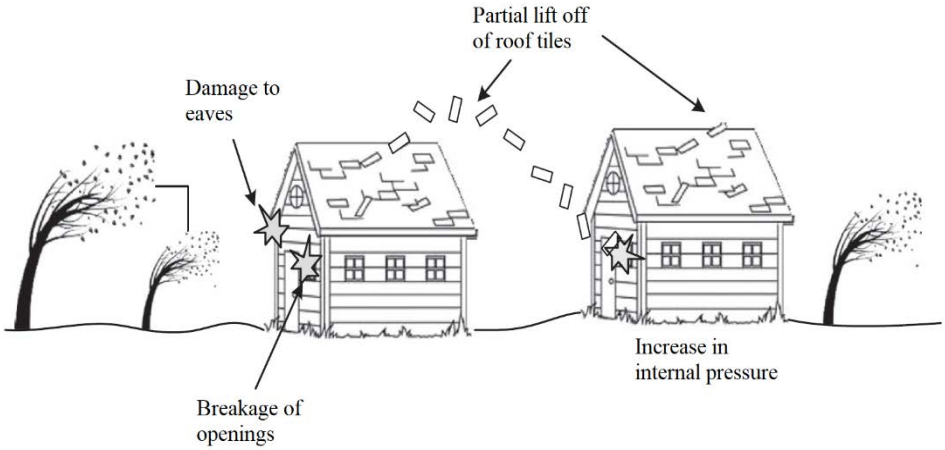

Figure 1 Windborne debris chain (from Kakimpa et al. (2012))

Due to their unpredictability and their danger, full-scale tornadoes are difficult to study, therefore it is particularly challenging to obtain in-situ velocity and pressure data. Using Doppler radar measurements, (Wurman and Alexander, 2005) collected wind field measurements of the Spencer South Dakota tornado of May 30, 1998. However, due to the earth's curvature and Doppler radar elevation angle, no data are usually obtained below 30m AGL (Wurman *et al.*, 2013), which is usually more than standard low-rise building heights. To overcome this limitation, Bluestein and Unruh (1989) used a Portable Doppler radar to intercept and get as close as 10km distance from a tornado. As a result, between 1995 and 2008, 150 tornadoes have been measured using Doppler On Wheels (DOWs) (Alexander and Wurman, 2008) with measurements within 20m Above Ground Level (AGL) (Kosiba and Wurman, 2013).

Recourse to physical modelling of tornadoes has had a significant impact in our understanding of the processes governing tornado-like flow fields. Ward (1972) pioneered the tornado generator that could generate realistic tornado-like vortices and sub-vortices. Ward-type generators use guide vanes to introduce angular momentum and an exhaust fan to generate an updraft. Several Ward-type generators were then developed to further investigate tornado-like vortices in small-scale (Church *et al.*, 1977), small/medium scale (Gillmeier *et al.*, 2018) and large-scale generators (Tang *et al.*, 2018). Over the past decades, tornado generators with new design have been developed: Mishra et al. (2008a; 2008b) developed a Ward-type generator where the circulation is driven by 16 slotted jets; (Haan *et al.*, 2008) developed a new large-scale translating generator with a central exhaust fan and an annular duct recirculating the flow downward; Refan et al. (2014) used the new large-scale 3D wind testing facility (WindEEE dome) to generate tornado-like vortices. Through the years and improvements, each generator presented improving similarities with full-scale tornadoes. The pressure drop in the vortex core matched with the 2004 Manchester (U.S.) tornado (Mishra *et al.*, 2008a) and velocity components showed good agreements with full-scale measurements (Haan *et al.*, 2008). Tornado-like vortex generators can also model one and two-cell vortices (Haan *et al.*, 2008; Tang *et al.*, 2018), and improved the understanding of the vortex breakdown during the transition between one and two-cell structure (Church and Snow, 1985). However, Baker and Sterling (2019) recently questioned the efficacy of tornado simulators to reproduce full-scale tornadoes. The authors looked at various dimensionless group to evaluate the performance of several tornado simulators with regards to dynamic, kinematic and geometric similarities. The

main conclusion drawn from this analysis is that some are able to match geometric similarity for some tornadoes, some are able to match kinematic similarity but none of the current tornado simulators are capable to show all similarities with full-scale tornadoes and therefore have limited capabilities.

Different analytical vortex models have been developed to reproduce tornado-like flow field (Rankine, 1882; Burgers, 1948; Rott, 1958; Sullivan, 1959; Baker and Sterling, 2017). However, due to the assumptions made and the complexity of tornado flow fields, some vortex models tend to only reproduce the tangential velocity component correctly and remain incapable of realistically modelling the radial and axial components. Gillmeier et al. (2018) compared vortex models with physically modelled flow fields and showed that Baker and Sterling's model is currently the most realistic on those cited above.

Debris flight models have also been developed, although they were originally simplified and only considered the drag forces (McDonald *et al.*, 1974) or the drag and lift forces (Lee, 1974). Subsequently, effort has been made to understand the forces involved during the flight of debris. As a result, Twisdale et al. (1979) performed an analysis of tornado missile transport using a 'random orientation 6-degree of freedom' 3D model including drag, lift and side forces; Tachikawa (1983, 1988) looked at the flight of flat plates in a wind-tunnel, resulting in the definition of the Tachikawa number (Holmes *et al.*, 2006) and accounting for the ratio of aerodynamic to gravity forces; Holmes (2004) and Holmes et al. (2006) developed debris flight equations for spherical and plate-type debris, respectively; Kordi and Kopp (2011) investigated the flight of windborne plate debris from a building in a wind-tunnel; Baker (2007) developed debris flight equations with a dimensionless approach. In a further paper, Baker and Sterling (2017) developed the debris flight equations for tornado-like wind field applications.

Although great effort has been undertaken over the past few decades to model and understand the flow field of a tornado, the flight of debris in a tornado flow field is still poorly understood. It is therefore not surprising that only a little can be found in the literature focusing on windborne debris flight in a tornado-like vortices (Sassa *et al.*, 2009; Maruyama, 2011; Noda *et al.*, 2013; Baker and Sterling, 2017). The current work presents an introductory overview of the experimental investigation of windborne debris flight in tornado-like flow field using a tornado generator and the Particle Tracking Velocimetry (PTV) technique and a methodology to compute debris trajectories using experimental data.

2 DEBRIS FLIGHT INVESTIGATION

2.1 *Experimental methodology*

2.1.1 *University of Birmingham Tornado-like Vortex Generator*

The University of Birmingham Tornado-like Vortex Generator (UoB-TVG) is a Ward-type generator used to investigate tornado-like vortices (Figure 2). A description of the generator can be found in Gillmeier et al. (2018) but for the sake of completeness a brief description is given below.

The generator consists of three different sections:

- a convergence chamber (1m height x 3.6m diameter) located at the bottom. 30 guide vanes equally spaced around the convergence chamber introduce angular momentum, and the vane angle (θ) can be set up from 0 degree, i.e. no swirling, to 70 degrees.
- a convection chamber (2m height x 3.1m diameter) sitting on top of the convergence chamber.
- a trapezoidal duct with 9 identical fans sitting on top on the convection chamber and generate the uplift through the updraft hole.

The updraft hole has a radius (r_0) of 0.5m and a honeycomb is placed to reduce secondary vortices from the fans interacting with the generated vortex (Ward, 1972). The fans generate a mean vertical velocity (W) of around 10 m/s at the top of the convection chamber, resulting in a radial Reynolds number ($Re_r = Wr_0/4\pi\nu$) of 5.4 x 10^4, with ν the kinematic viscosity of air. In the current work, the vane angle was set to 50 degrees for a resulting swirl ratio of 0.3. The swirl ratio is defined as a measure of the circulation strength relative to the updraft ($S = \tan\theta/2a$, with a the aspect ratio defined by the ratio of the inflow height h and the updraft radius r_0).

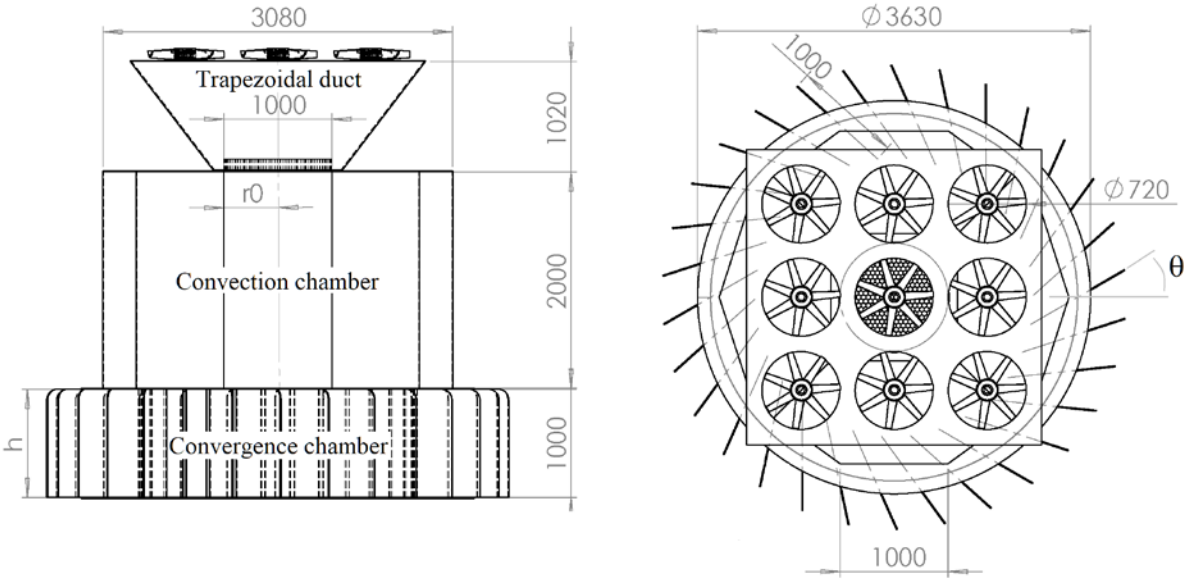

Figure 2 Schematic and dimensions of the University of Birmingham Tornado-like Vortex Generator (UoB-TVG).

2.1.2 *Wind velocity measurements*

The velocity flow field was measured using a TFI 4-hole Cobra probe (TFI, 2011). The Cobra can measure velocity data with magnitude higher than 2 m/s within a cone of influence of 45°. The probe was mounted on a two-axis traverse system located off-centre inside the generator and was held approximatively 0.7m away from the traverse system to minimalize disturbances. Point measurements were undertaken radially every 0.02m from the centre of the generator up to 0.5m and then every 0.04m up to 0.7m; and vertically every 0.02cm from 0.005m to 0.065m and then every 0.04m up to 0.425m. The point measurements were taken with a precision of less than 1mm. The velocity data were measured and averaged over a sampling duration of 82s and uncertainties are taken to be ±0.5m/s for the tangential velocity and ±0.2m/s for the radial and vertical velocity (Gillmeier *et al.*, 2018).

2.1.3 *3D Particle Tracking Velocimetry*

A full description of the 3D-PTV technique and development can be found in the literature (Maas *et al.*, 1993; Malik *et al.*, 1993). In the current work, the 3D-PTV system consists of three digital high-speed cameras, Sony NEX-FS700RH, used to record the motion of the compact debris. Two cameras are positioned at the top of the convection chamber and one camera at the top of the convergence chamber. The cameras were set up to record videos at 480 Hz at a resolution of 1920 × 1080 pixels. Four 50W LED lights were placed inside the chambers to illuminate the volume of interest. The cameras were synchronised using an ALE718 Multi Camera LANC controller, developed by Applied Logic Engineering, Inc. The cameras calibration is performed using a two-dimensional calibration target placed inside the UoB-TVG. A three-dimensional target was 3D printed and used to estimate the spatial uncertainties. The resulting root mean square errors in the x, y and z directions are 1.05mm, 1.20mm and 2.15 mm, respectively. The measurement volume in the x, y and z directions is approximately is 2 × 1.2 × 0.3 m, respectively. The digital images were pre-processed by substituting a mask from the images to filter background noises and to enhance the debris visibility. The data reduction was then performed using the open-source particle tracking software OpenPTV (OpenPTV, 2012). The output data were subsequently post-processed using MATLAB®.

2.1.4 *Compact debris and cubic model*

Spherical Styrofoam beads were used as compact debris in the current work. A particle size and shape analysis using ImageJ software was undertaken to characterise the distributions for a large set of sieved beads (around 3000 samples). The bead diameters were found to be between 1.6mm and 2.3mm, with a mean diameter of 1.94 ± 0.1mm and a circularity around 0.93.

In order to inject the debris inside the simulator, a seeding system was designed and built (Figure 3). It consists of a disc with 100 equidistant holes of 0.002m diameter connected to a stepper motor. The disc is enclosed into a chamber and rotates at a constant speed using a motor. A vent passing through the seeding system and aligned with the holes on the wheel allowed to inject 2mm Styrofoam beads into the simulator. The pressure difference between inside and under the simulator naturally sucked the spheres through the vent. The seeding

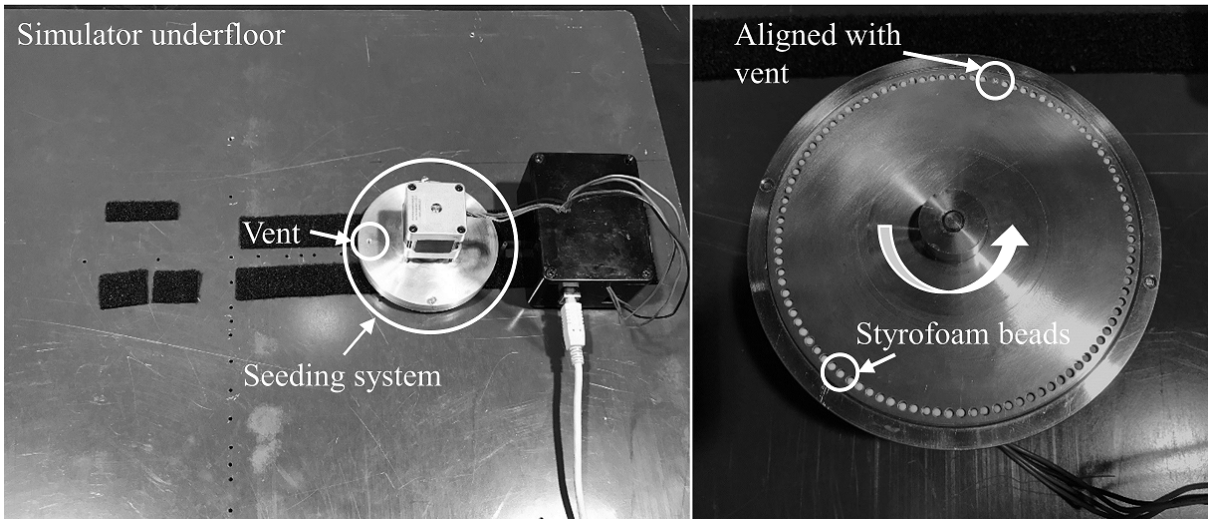

Figure 3 Seeding system used to inject debris into the simulator.

system was attached to the floor under the simulator and the vent was connected to the surface pressure taps. This allowed, as the motor rotates, to inject each individual particle at a time.

A low-rise building model (20mm sides length x 20mm height, Figure 4) was 3D printed and used to initiate debris flight from the building's roof. The building model has a geometric scale of 1/8 with regards to the size of the experimental core radius. Wurman et al. (2013) measured winds using a Doppler on Wheel radar during an F2 tornado and were able to determine the size of the tornado and debris cloud around it. The tornado was found to have a core radius of 100m with a debris cloud twice as large as the tornado core itself. Therefore, the building model would be equivalent to a building of around 13 × 13 × 13m at full-scale. In the current work, the building model is located at the core radius location and one hundred spheres (compact debris) were injected into the flow field from the top of it.

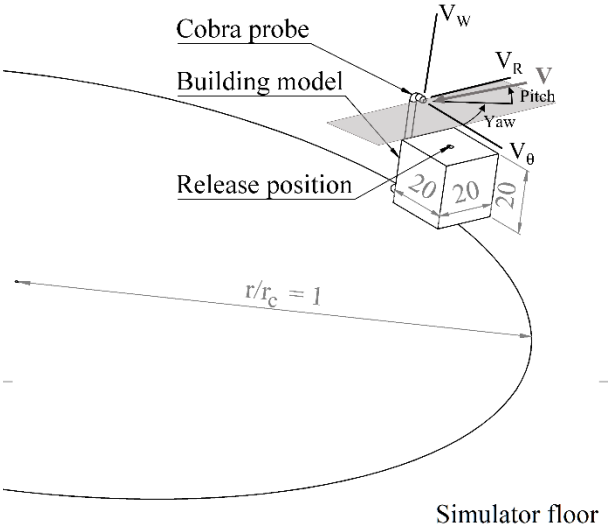

Figure 4 Building model and Cobra probe located at the core radius position. V_θ, V_R and V_W denote the wind tangential, radial, and vertical component, respectively, and **V** the wind velocity magnitude.

2.2 *Numerical methodology*

The 3D motion of Styrofoam beads in a tornado-like vortex was computed numerically to determine 3D trajectories, following a similar approach from Sassa et al. (2009). A compact debris with only drag forces acting and no rotation is assumed. The accelerations of the compact debris are defined as:

$$\frac{dV_{\theta,d}}{dt} = k\,\boldsymbol{V}\left(V_\theta - V_{\theta,d}\right) \tag{1}$$

$$\frac{dV_{R,d}}{dt} = k\,\boldsymbol{V}\left(V_R - V_{R,d}\right) \tag{2}$$

$$\frac{dV_{W,d}}{dt} = k\,\boldsymbol{V}\left(V_W - V_{W,d}\right) - g \tag{3}$$

where V_θ and $V_{\theta,d}$ are the local tangential wind and debris velocities respectively, k is a buoyancy parameter (Eq. 5), t represents the time, V_R and $V_{R,d}$ are the local radial wind and debris velocities respectively, V_W and $V_{W,d}$ are the local vertical wind and debris velocities respectively, and **V** is the vector of the relative velocity between the wind and debris defined as:

$$\boldsymbol{V} = \sqrt{\left(V_\theta - V_{\theta,d}\right)^2 + \left(V_R - V_{R,d}\right)^2 + \left(V_W - V_{W,d}\right)^2} \quad (4)$$

The buoyancy parameter (Holmes, 2004) is defined as:

$$k = \frac{\rho_{air}\, C_D}{2\, \rho_{debris}\, l} \quad (5)$$

where ρ_{air} is the air density, C_D the drag coefficient, ρ_{debris} the debris density and l the debris characteristic length. The parameters were set to ρ_{air} = 1.2 kg/m^3, C_D = 0.5, ρ_{debris} = 24 kg/m^3 and l = 2 d_{debris}/3, with d the debris diameter, giving a value of k = 9.5.

The velocity and position components, denoted hereafter with •, were computed numerically using a linear method as:

$$V_\bullet^{t+1} = V_\bullet^t + A_\bullet^t \Delta t \quad (6)$$

$$X_\bullet^{t+1} = X_\bullet^t + V_\bullet^t \Delta t \quad (7)$$

with Δt a timestep of 0.001s. A timestep of 0.001s offers a good ratio of stability/time efficiency considering the maximal wind velocities of the flow field used in the current work.

Experimental data were incorporated into the calculations, by incorporating the experimental wind and tracked data into the calculated accelerations (Eq. 1-4). For t=0, the initial conditions ($V_\bullet^0$ and $X_\bullet^0$) were set to the velocity and position data obtained from the particle tracking experiment (Eq. 6-7). To determine at each timestep the wind velocities to be incorporated into the calculations, bilinear interpolation was used to interpolate sub-grid velocities from the positions $X_\bullet^t$. Since the measurement grid was coarse, this technique improves the accuracy and robustness of the calculations by interpolating wind velocities rather than finding the closest measured point. The modelling of the debris trajectory was stopped when the debris first impacts the ground.

3 RESULTS

3.1 *Tornado wind field*

Figure 5 shows the 3D velocity flow field and radial profile of the velocity components at the lowest height measured (z/r_c = 0.03) in the UoB-TVG for a swirl ratio of 0.3. Heights and radial positions are normalised by the core radius r_c, located at r/r_c = 1, and velocities are normalised by the maximal tangential velocity $V_{\theta,max}$. The core radius was estimated as the radius where the maximal tangential velocity occurs and was found to be equal to 0.144m. Figure 5 (a) shows the complexity of a tornado-like flow field, with a strong inflow in the lower level towards the vortex core region and a strong updraft at the corner region (r/r_c = 1). The strong tangential velocity region located at the core radius region, the core radius increase with height, as well as the positive radial inflow inside the vortex core are consistent with previous work undertaken by Haan et al. (2008), Gillmeier et al. (2018) and Tang et al. (2018). The recirculation located at z/r_c =1 and r/r_c = 2 seems to indicate the presence of a vortex breakdown, which would indicate that for S=0.3 the tornado flow field is not yet fully developed into a two-cell vortex. Vortex wandering characterisation (not shown here) revealed that for the current swirl ratio,

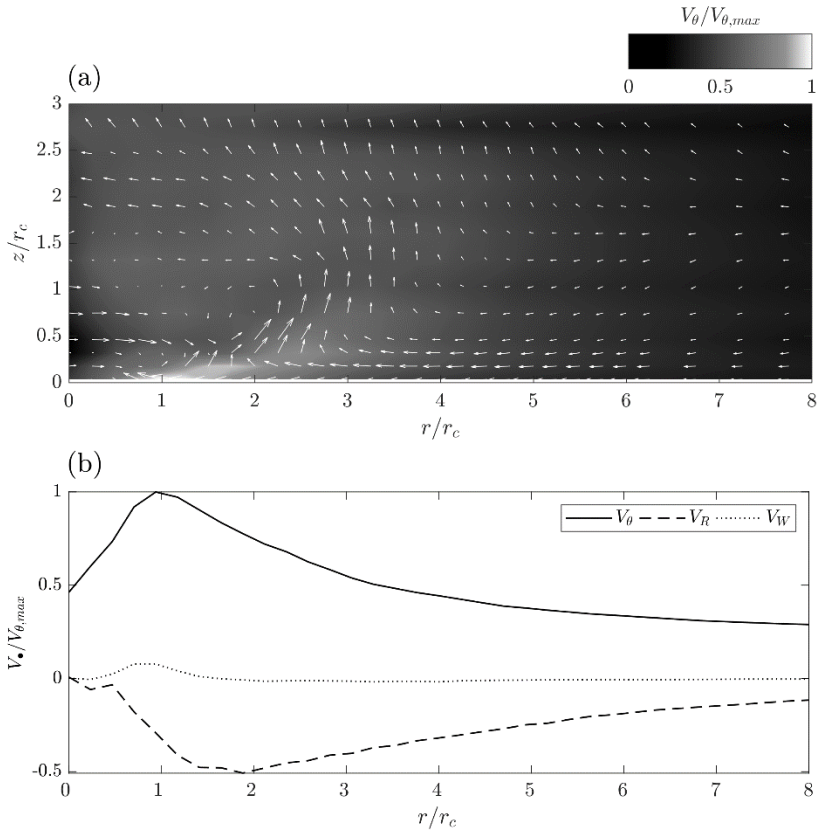

Figure 5 (a) 3D velocity field for S=0.3. Contour denotes the tangential velocity and the vectors denote the velocity vector between radial and vertical velocity. (b) Velocity components for the lowest height (5mm), located in the boundary-layer.

the vortex typically wanders around the centre of the simulator up to $0.15r_c$. Overall, the vortex structure shows a relatively good agreement with previous work from Gillmeier et al. (2018) and the VorTECH generator for a similar swirl ratio (Tang *et al.*, 2018). Figure 5 (b) shows the tangential, radial and vertical velocity profiles for the lowest height measured and accounts for a tangential velocity increasing until the core radius r_c, a strong radial inflow up (negative radial velocities) to half the maximum tangential velocity ($V_R/V_{\theta,max} = 0.44$) at $r/r_c = 2$ and a weak updraft around the core radius location.

Figure 6 shows the vertical profiles of velocities closed to the ground at the core radius location with and without building model included. To measure the vertical profile on top of the model, the Cobra probe's head was mounted under the simulator at the core radius location. The probe's head was placed perpendicular to core centre's direction and at the building model's corner between the top and leeward side, as shown in Figure 4. With no building model, the tangential velocity (Figure 6 (a)) at this location is similar in many respects to a typical boundary-layer profile. The radial velocity (Figure 6 (b)) is predominantly negative over the height and accounts for the radial inflow as found in Figure 5. The vertical velocity (Figure 6 (c)) shows a change of sign at around $z/r_c = 0.05$ which is difficult to interpret since the velocity remains relatively close to zero and the measurement is taken in a turbulent region. When the building model was included, the profile was measured from the top of the leeward side, to be as close as possible from the debris release position. It shows that the tangential velocity is typically not affected with height by the building model (Figure 6 (a)), and that the radial and vertical velocities are reduced in magnitude but still display a similar profile with height

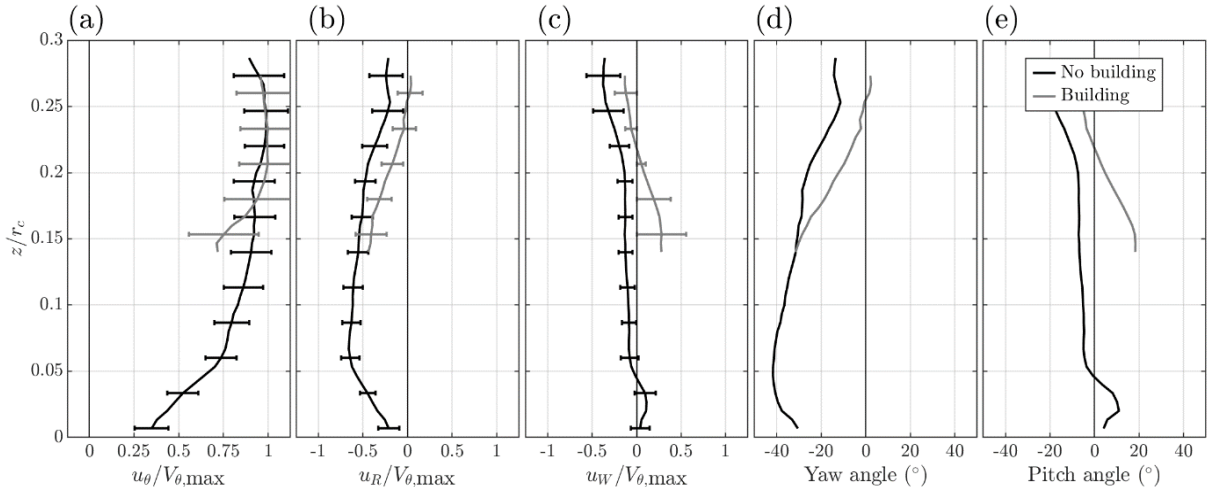

Figure 6 Vertical velocity profiles of normalised – (a) tangential, (b) radial, (c) vertical velocity, respectively, (d) yaw angle and (e) pitch angle. The black line denotes when the building model is not included into the flow field, and the grey line when it is included. The horizontal capped lines denote the measurement uncertainties. The yaw angle denotes the horizontal angle between the tangential and radial velocities and the pitch angle the vertical angle with regard to the horizontal plane.

(Figure 6 (b and c)). The largest discrepancies observed around $z/r_c = 0.15$ are associated with a potential flow separation occurring on top the building model. Numerical simulations of a low-rise building in tornado-like flow field with a similar swirl ratio (S=0.4) showed that a recirculation is generated on the lee-ward side of the building (Nasir, 2017). That recirculation produces a downward flow in the wake of the building which most likely explain the debris behaviour described in the following section. The yaw angle (Figure 6 (d)) refers to the horizontal wind direction facing the probe while the pitch angle (Figure 6 (e)) refers to the vertical wind direction.

3.2 *Example of 3D trajectories from a low-rise building*

Figure 7 illustrates an example of 3D debris trajectories initiated from the top of a low-rise building located at the core radius location and obtained using 3D-PTV. It shows that the debris are initiated with different horizontal and vertical directions resulting in a large spread of the falling locations. Further interpretation and analysis are discussed in the following section.

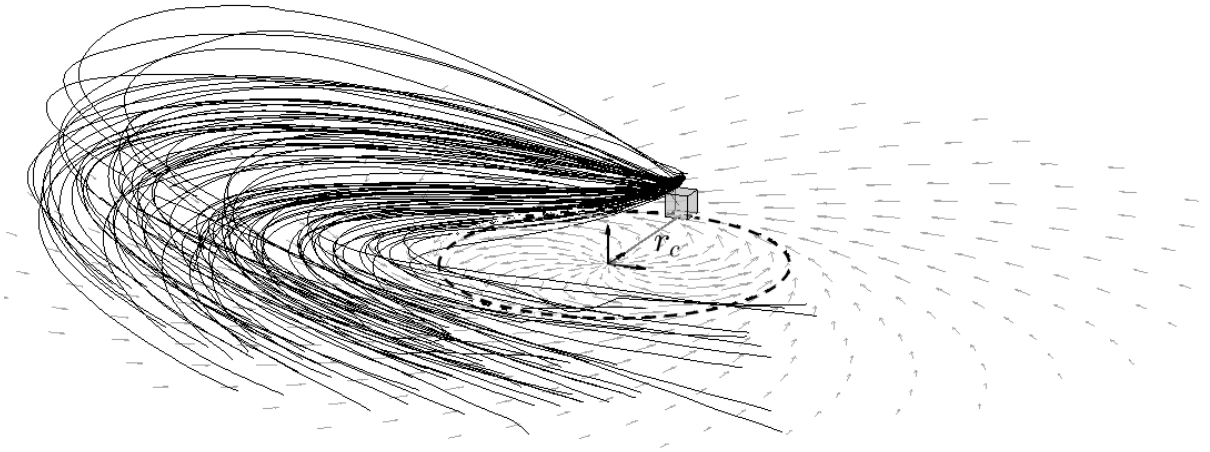

Figure 7 3D representation of the flight of debris from a low-rise building at the core radius (r_c) location. The dash line denotes the size the core radius, the arrows denotes the idealised flow-field at building height.

3.3 *Comparison of debris flight trajectories with no building and a building included*

The comparison between different debris flight configurations is shown in Figure 8. The debris trajectories obtained experimentally are shown in Figure 8 (a and c), while Figure 8 (b and d) show the numerical reproduction of these trajectories. In both cases, visual similarities are observed and are quantified in Figure 10. Figure 8 (a and c) illustrate the typical set of experimental data obtained using 3D-PTV when injecting 100 particles from the core radius position. Similar trajectory behaviours were found in the literature, although studied numerically, when debris were released from the core radius location (Maruyama, 2011; Noda *et al.*, 2013). In the present cases, the debris were injected from the floor simulating the initiation of debris flight in a landscape environment (i.e. no building), and from the top of a building. The tracking was stopped when the particles impacted the ground after being airborne to reflect what could be observed during a full-scale event. However, it is worth noting that due to the elasticity of the Styrofoam bead, its light mass and the smooth floor surface in the tornado generator, the beads bounce when falling to the ground. For the sake of the current analysis, such motion has been neglected and is not considered further.

Figure 8 (a) shows that the particles are ejected outward from the vortex following a relatively straight line for a short period of time. The particles are then swirling back again around the vortex before falling to the ground. It also illustrates that a slight variation of the early stage trajectories can result in a large variation of the impact location. The variability in the early stage trajectories observed in the trajectories could be due to the varying size of the beads, although it is most likely that the variation is due to the vortex wandering and/or to turbulent fluctuations of the local wind field. Figure 8 (c) shows the debris trajectories when injected

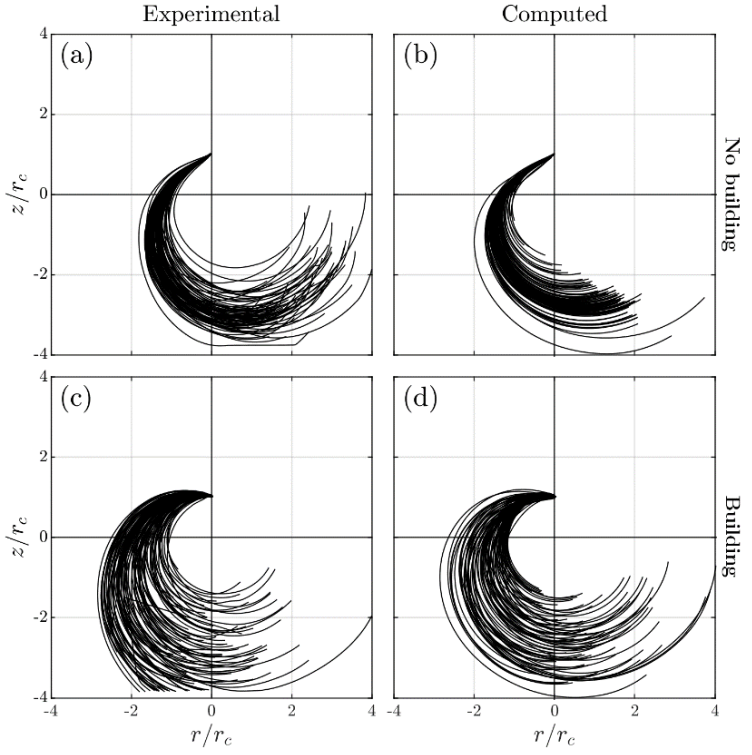

Figure 8 Top view of experimental and numerical debris trajectories. Left column denotes the experimental trajectories (a-c), right column the computed trajectories (b-d). The top row denotes the trajectories when the building model is not included (a-b), the bottom row the trajectories when the building model is included (c-d).

from the top of the cubic model. It illustrates a greater variation of the early stage trajectories than without the model resulting in a larger region where the debris falls. The larger variation can be attributed to the disturbance of the local flow field around the building model. This assumption can be supported by the initial velocity distributions, i.e. the first debris velocities calculated using 3D-PTV (Figure 9). It appears that debris are driven by positive tangential velocities in both situations (Figure 9 (a)), however radial and vertical velocities have opposite sign between the two. As a result, an overall difference of 40 degrees in direction can be noticed when including the building into the flow field (Figure 9 (d)). Furthermore, Figure 9 (c) shows that debris are mainly driven by both positive and negative vertical velocities when released from the top of the building, which could be explained by a potential flow separation. When debris are driven by negative vertical velocity, the debris falls quickly to the ground and is travelling longer distances due to strong local tangential velocities, and therefore accounts for the closest trajectories to the vortex core. On the other hand, the debris tends to be ejected outward the core and to fall at even longer distances away from the core radius. This behaviour is visually observed in Figure 7. Therefore, the risks with windborne debris initiated from a low-rise building are not only associated with long-range falling debris but also with possible short-range impacts at higher velocities.

Figure 8 (b and d) presents the computed debris trajectories using experimental wind and tracking data. In both cases, the computed trajectories are in good agreement with the tracked trajectories. Although the flow field is assumed axisymmetric and does not include any turbulence, it shows that the present methodology can reproduce the trajectories variability. Table 1 compares the components of wind and initial debris velocities and shows that when the building is not included, the velocity components are matching wind and debris. This validates the assumption that variability in debris flight is mainly a wind-driven process. When

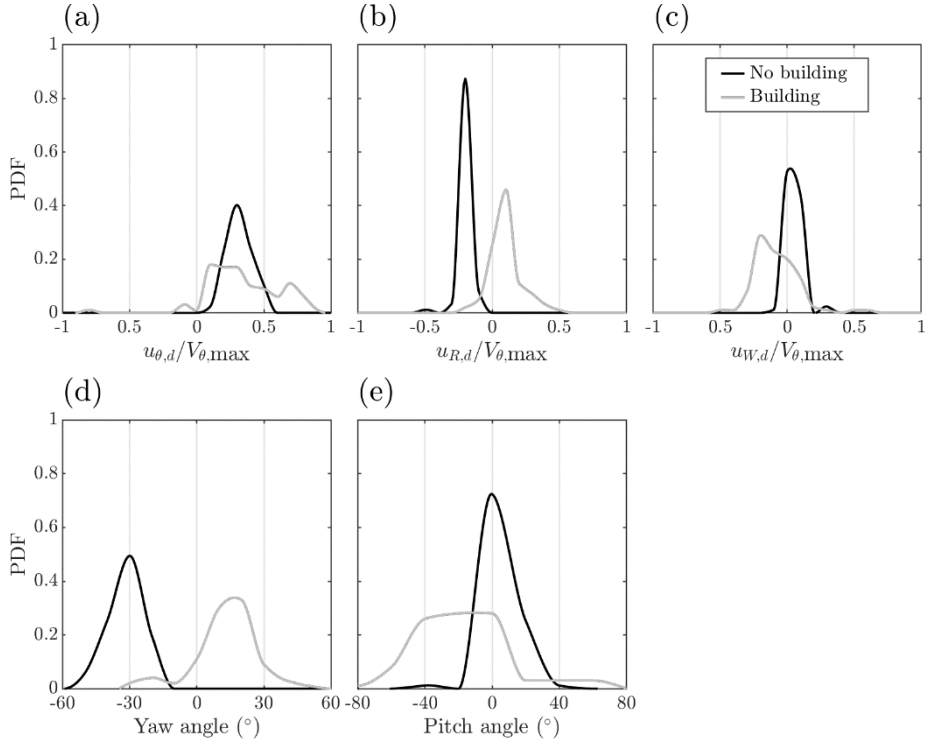

Figure 9 Distribution of debris initial tangential (a), radial (b), vertical (c) velocities, yaw (d) and pitch (e) angle, when the low-rise building model is and is not included in the tornado-like flow field.

the building is included, large discrepancies are observed between wind and debris which could be explained by the fact that velocities are not measured exactly at the same position.

Table 1 Comparison between wind and initial debris velocities, pitch and yaw angles, when the building model was included and not included in the simulations.

		$u_\theta / V_{\theta,max}$	$u_R / V_{\theta,max}$	$u_W / V_{\theta,max}$	Pitch (°)	Yaw (°)
No building	Wind	0.30	-0.20	0.04	25.8	4.10
	Debris	0.27	-0.16	0.04	30.7	7.10
Building	Wind	0.70	-0.44	0.27	-32.1	17.7
	Debris	0.38	0.11	-0.09	-16.7	-17.3

Figure 10 shows the debris flight analysis with normalised flight parameters determined from the debris trajectories (Figure 8). The flight distance (Figure 10 (a)) accounts for the cumulative distance travelled by a debris, the flight time (Figure 10 (b)) the duration while the debris is airborne, V_{max} (Figure 10 (c)) the maximal velocity reached by the debris, and flight time to V_{max} (Figure 10 (d)) the duration taken by a debris to reach the maximal velocity. Overall, it shows that including a building model does not affect the flight behaviour of the debris significantly. This corroborates the assumption that the overall flow field is not affected by the building model, as shown in Figure 6. The numerical simulations tend to reproduce some behaviour, although more variability is generally observed. The flight distance shows good agreement with experimental results and coincides with the debris trajectories overall behaviour (Figure 8), as does the flight time. However, the numerical simulations show limitations in modelling the maximum velocity V_{max}, and therefore the flight time to reach V_{max} (Figure 10 (c and d)). This could be explained by the flow field variability (due to wandering and/or turbulence) that is diminished after averaging and could result in a stronger instantaneous flow field at the time of the experiment.

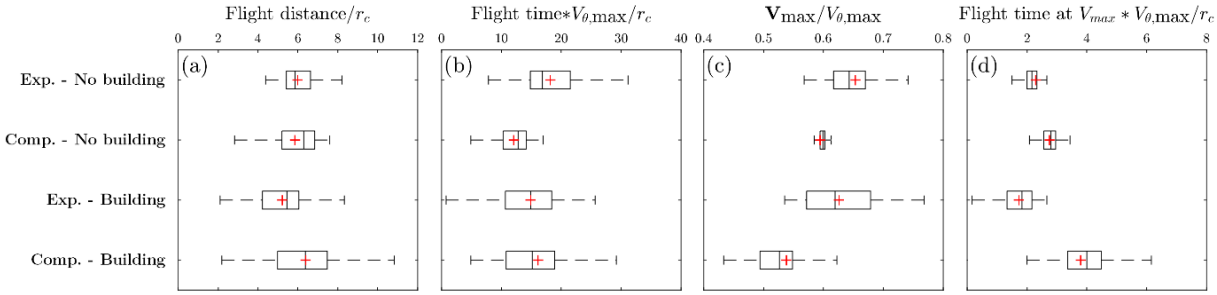

Figure 10 Debris flight analysis – the red cross denotes the mean value, the box interquartile range, the vertical line the median and the whiskers the range from minimal to maximal values.

4 CONCLUDING REMARKS

In this work, physical and numerical simulations were used to investigate the flight of debris in tornado-like vortices initiated with and without a low-rise building model. A medium-range vortex was simulated in a tornado-like vortex generator with a swirl ratio of 0.3. Wind measurements displayed a complex flow field with a strong tangential velocity in the corner region of the vortex, and strong radial inflow outside the vortex core. Vertical profiles of winds show that overall, the time-averaged flow field is not significantly affected by included a low-rise building model but tends to reduce in magnitude of the radial and vertical velocities with height. The current study focused on releasing Styrofoam beads in a tornado-like flow field and investigates the effect of releasing the debris from the top of the building model. Debris trajectories with and without the building model included show differences in early stage trajectory behaviors. When the building model is not included, trajectories follow a narrower path in early-stage flight with respect to the mean local flow field direction. When the building model is included, the early-stage debris trajectories have a different main direction with more variability resulting in a wider falling region. However, the analysis of different characteristic flight parameters shows good agreement between the two situations. It confirms that in the present case the overall flow field in a tornado-like vortex is not affected by including a building model; however, the local flow field in the proximity of the model is affected. Numerical calculations were used to simulate the debris trajectories and flight behaviour. Using debris flight equations with wind and tracked experimental data, the computed trajectories show strong similarities with experimental trajectories. The debris flight analysis shows that the simulations could reproduce the overall trajectories but had limitations in simulating maximum velocities. The limitations could be attributed to the experimental wind data used to compute the trajectories and not necessarily to the methodology itself. Finally, this numerical methodology presents advantages to investigate debris flight in tornadoes:

- Gillmeier et al. (2018) showed that analytical vortex models can reproduce some of the behaviours observed in full scale and modelled tornadoes but fail to reproduce the complexity of the 3D flow field. Wind measurements help describing the complexity that models fail to reproduce and therefore integrate a more “realistic” flow field to the study of debris flight.
- Using bilinear interpolation to better approximate the local wind field increases the accuracy of the computed positions and velocities and does not require a fine measurement grid. It also significantly reduces the computation time and does not require high computational power.
- The methodology also allows any type of debris in tornado-like flow field to be studied. By adjusting the debris flight equations to either compact (Holmes, 2004) or plate (Holmes *et al.*, 2006), a large range of debris type, size and density (i.e. Tachikawa number) could be investigated.
- The methodology could also be applied to full-scale tornado wind data, however, Doppler radars often fail to measure wind below 30m AGL (Wurman *et al.*, 2013), which is where most of debris are becoming airborne and impacting structures. When data becomes available, comparison and validation could be undertaken at full-scale.

Although the methodology has many advantages, it also has limitations. The assumption of an axisymmetric flow field does not reflect the complexity of a tornado-like flow field. Volumetric wind measurements using neutral buoyancy tracers and laser illumination (Tomographic PIV, 3D-PTV, etc.) could help retrieving instantaneous 3D flow field. Finally, the methodology only considers averaged flow fields. Turbulence could be incorporated into the simulation (Holmes, 2004) to recreate wind field fluctuations but would require a better understanding of the turbulence in tornadoes/tornado-like vortices.

5 ACKNOLEDGMENTS

This paper was previously submitted and published in the proceedings of the 15th International Conference of Wind Engineering (ICWE15), Beijing, China. The authors wish to thank the organising and scientific committee for the financial support and opportunity to present this paper at the ICWE15.

6 REFERENCES

Alexander, C. R. and Wurman, J. (2008) 'Updated mobile radar climatology of supercell tornado structures and dynamics', in *24th Conf. on Severe Local Storms, Savannah, GA, Amer. Meteor. Soc.*, p. 19.4.

Baker, C. J. (2007) 'The debris flight equations', *Journal of Wind Engineering and Industrial Aerodynamics*, 95(5), pp. 329–353. doi: 10.1016/j.jweia.2006.08.001.

Baker, C. J. and Sterling, M. (2017) 'Modelling wind fields and debris flight in tornadoes', *Journal of Wind Engineering and Industrial Aerodynamics*, 168(February), pp. 312–321. doi: 10.1016/j.jweia.2017.06.017.

Baker, C. and Sterling, M. (2019) 'Are Tornado Vortex Generators fit for purpose?', *Journal of Wind Engineering and Industrial Aerodynamics*, 190, pp. 287–292. doi: https://doi.org/10.1016/j.jweia.2019.05.011.

Bluestein, H. B. and Unruh, W. P. (1989) 'Observations of the Wind Field in Tornadoes, Funnel Clouds, and Wall Clouds with a Portable Doppler Radar', *Bulletin of the American Meteorological Society*. American Meteorological Society, 70(12), pp. 1514–1525. doi: 10.1175/1520-0477(1989)070<1514:OOTWFI>2.0.CO;2.

Brooks, H. E. and Doswell, C. A. (2001) 'Normalized Damage from Major Tornadoes in the United States: 1890–1999', *Weather and Forecasting*. American Meteorological Society, 16(1), pp. 168–176. doi: 10.1175/1520-0434(2001)016<0168:NDFMTI>2.0.CO;2.

Burgers, J. M. (1948) 'A Mathematical Model Illustrating the Theory of Turbulence', in Von Mises, R. and Von Kármán, T. B. T.-A. in A. M. (eds). Elsevier, pp. 171–199. doi: https://doi.org/10.1016/S0065-2156(08)70100-5.

Church, C. R. and Snow, J. T. (1985) 'Measurements of Axial Pressures in Tornado-like Vortices', *Journal of the Atmospheric Sciences*, 42(6), pp. 576–582. doi: 10.1175/1520-0469(1985)042<0576:MOAPIT>2.0.CO;2.

Church, C. R., Snow, J. T. and Agee, E. M. (1977) 'Tornado Vortex Simulation at Purdue University', *Bulletin of the American Meteorological Society*. American Meteorological Society, 58(9), pp. 900–909. doi: 10.1175/1520-0477(1977)058<0900:TVSAPU>2.0.CO;2.

Gillmeier, S. *et al.* (2018) 'A reflection on analytical tornado-like vortex flow field models', *Journal of Wind Engineering and Industrial Aerodynamics*, 174, pp. 10–27. doi: https://doi.org/10.1016/j.jweia.2017.12.017.

Haan, F. L., Sarkar, P. P. and Gallus, W. A. (2008) 'Design , construction and performance of a large tornado simulator for wind engineering applications', 30, pp. 1146–1159. doi: 10.1016/j.engstruct.2007.07.010.

Holmes, J. D. (2004) 'Trajectories of spheres in strong winds with application to wind-borne debris', *Journal of Wind Engineering and Industrial Aerodynamics*, 92(1), pp. 9–22. doi: https://doi.org/10.1016/j.jweia.2003.09.031.

Holmes, J. D., Baker, C. J. and Tamura, Y. (2006) 'Tachikawa number: A proposal', *Journal of Wind Engineering and Industrial Aerodynamics*, 94(1), pp. 41–47. doi: https://doi.org/10.1016/j.jweia.2005.10.004.

Kakimpa, B., Hargreaves, D. M. and Owen, J. S. (2012) 'An investigation of plate-type windborne debris flight using coupled CFD–RBD models. Part I: Model development and

validation', *Journal of Wind Engineering and Industrial Aerodynamics*, 111, pp. 95–103. doi: https://doi.org/10.1016/j.jweia.2012.07.008.

Kordi, B. and Kopp, G. A. (2011) 'Effects of initial conditions on the flight of windborne plate debris', *Journal of Wind Engineering and Industrial Aerodynamics*, 99(5), pp. 601–614. doi: https://doi.org/10.1016/j.jweia.2011.02.009.

Kosiba, K. A. and Wurman, J. (2013) 'The Three-Dimensional Structure and Evolution of a Tornado Boundary Layer', *Weather and Forecasting*. American Meteorological Society, 28(6), pp. 1552–1561. doi: 10.1175/WAF-D-13-00070.1.

Lee, A. J. H. (1974) 'A general study of tornado-generated missiles', *Nuclear Engineering and Design*, 30(3), pp. 418–433. doi: https://doi.org/10.1016/0029-5493(74)90227-1.

Maas, H. G., Gruen, A. and Papantoniou, D. (1993) 'Particle tracking velocimetry in three-dimensional flows', *Experiments in Fluids*, 15(2), pp. 133–146. doi: 10.1007/BF00190953.

Malik, N. A., Dracos, T. and Papantoniou, D. A. (1993) 'Particle tracking velocimetry in three-dimensional flows', *Experiments in Fluids*, 15(4), pp. 279–294. doi: 10.1007/BF00223406.

Maruyama, T. (2011) 'Simulation of flying debris using a numerically generated tornado-like vortex', *Journal of Wind Engineering and Industrial Aerodynamics*, 99(4), pp. 249–256. doi: https://doi.org/10.1016/j.jweia.2011.01.016.

McDonald, J. R., Mehta, K. C. and Minor, J. E. (1974) 'Tornado-resistant design of nuclear power-plant structures', *Nucl Safety*. United States, 15(4), pp. 432–439.

Mishra, Amit R, James, D. L. and Letchford, C. W. (2008) 'Physical simulation of a single-celled tornado-like vortex , Part A : Flow field characterization', 96, pp. 1243–1257. doi: 10.1016/j.jweia.2008.02.063.

Mishra, A R, James, D. L. and Letchford, C. W. (2008) 'Physical simulation of a single-celled tornado-like vortex , Part B : Wind loading on a cubical model', 96, pp. 1258–1273. doi: 10.1016/j.jweia.2008.02.027.

Mulder, K. J. and Schultz, D. M. (2015) 'Climatology, Storm Morphologies, and Environments of Tornadoes in the British Isles: 1980–2012', *Monthly Weather Review*. American Meteorological Society, 143(6), pp. 2224–2240. doi: 10.1175/MWR-D-14-00299.1.

Nasir, Z. (2017) *Numerical modeling of tornado-like vortex and its interaction with bluff-bodies*. The University of Western Ontario.

Noda, M. *et al.* (2013) 'Behavior of Flying Debris in Tornado-like Flow', *Journal of Wind Engineering*, 38(3), pp. 63–73. doi: 10.5359/jwe.38.63.

OpenPTV (2012) *What is Open source Particle Tracking Velocimetry*. Available at: https://www.openptv.net/.

Rankine, W. J. M. (1882) *A Manual of Applied Physics*. 10th edn. Charles Griff and Co.

Refan, M., Hangan, H. and Wurman, J. (2014) 'Journal of Wind Engineering Reproducing tornadoes in laboratory using proper scaling', *Journal of Wind Engineering and Industrial Aerodynamics*. Elsevier, 135, pp. 136–148. doi: 10.1016/j.jweia.2014.10.008.

Rott, N. (1958) 'On the viscous core of a line vortex', *Zeitschrift für angewandte Mathematik und Physik 9*, pp. 543–553.

Sassa, K., Takemura, S. and Yamashita, K. (2009) 'The behaviour of windborne debris accompanied by a traveling', in *7th Asia-Pacific Conference on Wind Engineering, APCWE-VII Asia-Pacific Conference on Wind Engineering*.

Sullivan, R. D. (1959) 'A Two-Cell Vortex Solution of the Navier-Stokes Equations', *Journal of the Aerospace Sciences*. American Institute of Aeronautics and Astronautics, 26(11), pp. 767–768. doi: 10.2514/8.8303.

Tachikawa, M. (1983) 'Trajectories of flat plates in uniform flow with application to wind-generated missiles', *Journal of Wind Engineering and Industrial Aerodynamics*, 14(1), pp. 443–453. doi: https://doi.org/10.1016/0167-6105(83)90045-4.

Tachikawa, M. (1988) 'A method for estimating the distribution range of trajectories of wind-borne missiles', *Journal of Wind Engineering and Industrial Aerodynamics*, 29(1), pp. 175–184. doi: https://doi.org/10.1016/0167-6105(88)90156-0.

Tang, Z. *et al.* (2018) 'Characteristics of Tornado-Like Vortices Simulated in a Large-Scale Ward-Type Simulator', *Boundary-Layer Meteorology*. Springer Netherlands, 166(2), pp. 327–350. doi: 10.1007/s10546-017-0305-7.

TFI (2011) *Turbulent Flow Instrumentation - Cobra Probe - Getting started guide. Technical report, Turbulent Flow Instrumentation*.

Twisdale, L. A., Dunn, W. L. and Davis, T. L. (1979) 'Tornado missile transport analysis', *Nuclear Engineering and Design*, 51(2), pp. 295–308. doi: https://doi.org/10.1016/0029-5493(79)90096-7.

Ward (1972) 'The exploration of certains features of tornado dynamics using a laboratory model'.

Ward, N. B. (1972) 'The Exploration of Certain Features of Tornado Dynamics Using a Laboratory Model', *Journal of the Atmospheric Sciences*. American Meteorological Society, 29(6), pp. 1194–1204. doi: 10.1175/1520-0469(1972)029<1194:TEOCFO>2.0.CO;2.

Wurman, J. and Alexander, C. R. (2005) 'The 30 May 1998 Spencer, South Dakota, Storm. Part II: Comparison of Observed Damage and Radar-Derived Winds in the Tornadoes', *Monthly Weather Review*. American Meteorological Society, 133(1), pp. 97–119. doi: 10.1175/MWR-2856.1.

Wurman, J., Kosiba, K. and Robinson, P. (2013) 'In Situ, Doppler Radar, and Video Observations of the Interior Structure of a Tornado and the Wind–Damage Relationship', *Bulletin of the American Meteorological Society*. American Meteorological Society, 94(6), pp. 835–846. doi: 10.1175/BAMS-D-12-00114.1.